PROCEEDINGS A

royalsocietypublishing.org/journal/rspa

Review

Cite this article: Ali SZ, Dey S. 2019 Bed particle saltation in turbulent wall-shear flow: a review. *Proc. R. Soc. A* **475**: 20180824.
http://dx.doi.org/10.1098/rspa.2018.0824

Received: 22 November 2018
Accepted: 28 January 2019

Subject Areas:
fluid mechanics, geophysics, mathematical modelling

Keywords:
turbulent wall-shear flow, bed particle saltation, bedload transport

Authors for correspondence:
Sk Zeeshan Ali
e-mail: skzeeshanali@iitkgp.ac.in
Subhasish Dey
e-mail: sdey@iitkgp.ac.in

Bed particle saltation in turbulent wall-shear flow: a review

Sk Zeeshan Ali[1] and Subhasish Dey[1,2,3]

[1]Department of Civil Engineering, Indian Institute of Technology Kharagpur, Kharagpur 721302, West Bengal, India
[2]Physics and Applied Mathematics Unit, Indian Statistical Institute, Kolkata 700108, West Bengal, India
[3]Department of Hydraulic Engineering, State Key Laboratory of Hydro-Science and Engineering, Tsinghua University, Beijing 100084, People's Republic of China

SZA, 0000-0003-0763-7437; SD, 0000-0001-9764-1346

Bed particle saltation in turbulent wall-shear flow remains an intriguing phenomenon in applied hydrodynamics. In this review, we report the current state of the art of bed particle saltation in turbulent wall-shear flow, highlighting the physical characteristics of bed particle saltation and its mathematical modelling. A critical appraisal of the mechanics of bed particle saltation is presented thorough ample experimental evidence. The salient features of bed particle saltation, encompassing the saltation height, saltation length, particle velocity, saltation duration, particle collision with the bed, particle rotation, particle resting time and particle re-entrainment, are thoroughly discussed. Both the deterministic and computational fluid dynamics approaches in modelling bed particle saltation are summarized, and the subtle role of the hydrodynamic forces is elaborated. The estimation of bedload flux in a fluvial environment, emanating from the mathematical modelling of bed particle saltation, is delineated using different modelling approaches. Finally, the challenges in modelling bed particle saltation are highlighted, and a new look at bed particle saltation is furnished.

1. Introduction

In classical geomorphology and applied hydrodynamics, the term *saltation*, consonant with its etymological meaning, refers to the intermittent leaping of bed

THE ROYAL SOCIETY PUBLISHING

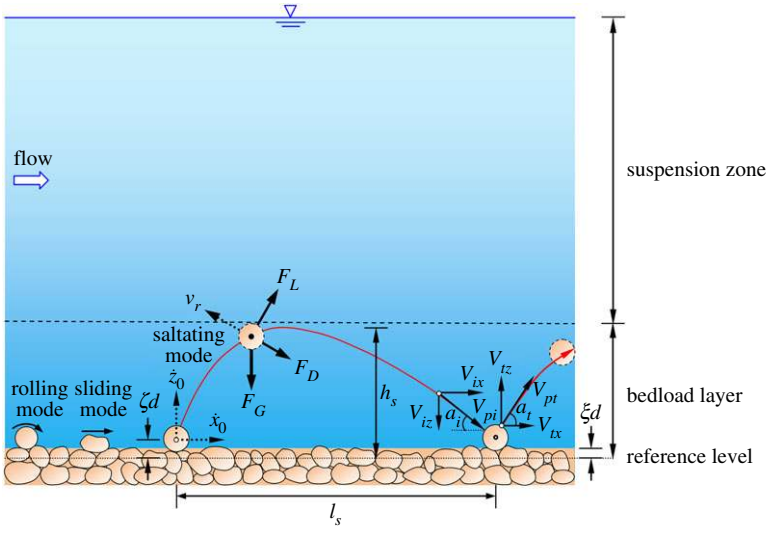

Figure 1. Bed particle saltation with representative particle size d, saltation height h_s and saltation length l_s. The reference level is located at a distance ξ_d below the summitof bed particles. Here, F_D is the hydrodynamic drag, F_L is the hydrodynamic lift, F_G is the submerged weight of the particle and v_r is the particle velocity relative to the fluid flow. The initial position of the saltating particle lying on the closely packed bed particles is at a distance ζd above the reference level and $(\dot{x}_0, \dot{z}_0)$ are the initial particle velocity components at the beginning of particle motion. In addition, $V_{pi}[= (V_{ix}, V_{iz})]$ and $V_{pt}[= (V_{tx}, V_{tz})]$ are the particle incidence and take-off velocities at collision, and a_i and a_t are the particle incidence and take-off angles at collision, respectively. (Online version in colour.)

particles by the action of a flowing fluid. Bed particle saltation is one of the fascinating manifestations of turbulent wall-shear flow over a loose granular bed. It plays a subtle role in governing the morphological print of terrestrial topography by transporting and depositing bed particles. It appears ubiquitously in a wide variety of fluvial and aeolian environments; for instance, in rivers, deserts and many others [1–9]. In addition, the existence of bed particle saltation has been evidenced on other planetary topographies [10–12].

In a turbulent wall-shear flow over a loose granular bed, when the applied bed shear stress τ_0 slightly exceeds its threshold value τ_{0c}, called the *threshold bed shear stress* for the initiation of bed particle motion, the particles roll and/or slide in contact with the bed (figure 1). As the applied bed shear stress increases further owing to an increase in flow velocity, the particles move along the bed, performing a series of brief jumps of approximately identical steps, called *saltation* [13]. Bed particle saltation is limited to a thin *bedload layer*, within which the particles are collectively transported in rolling, sliding and saltating modes, called *bedload transport*. Beyond the bedload layer, known as the *suspension zone* (figure 1), the particles are primarily transported in suspension mode, the physical mechanism of which has been reviewed elsewhere [14,15]. In this review, we shed light specifically on bed particle saltation, which remains a predominating contributor to bedload transport. Bed particle saltation is principally governed by hydrodynamic drag F_D and lift F_L forces (figure 1). When a bed particle is lifted off the bed by a hydrodynamic force to a certain height, it begins to descend and finally returns to the bed under the action of gravity. In figure 1, h_s denotes the saltation height, representing the distance from the particle centroid at the pinnacle of the particle trajectory to a reference level ($z = 0$). The reference level is considered to be a distance of ξd below the summit of the bed particles, where d is the median particle size. In addition, l_s represents the saltation length, which is the distance between the initial and final positions of the particle centroid during a saltation step. The initial position of the saltating particle resting on bed particles is considered to be $z = \zeta d$. The subsequent step of bed particle

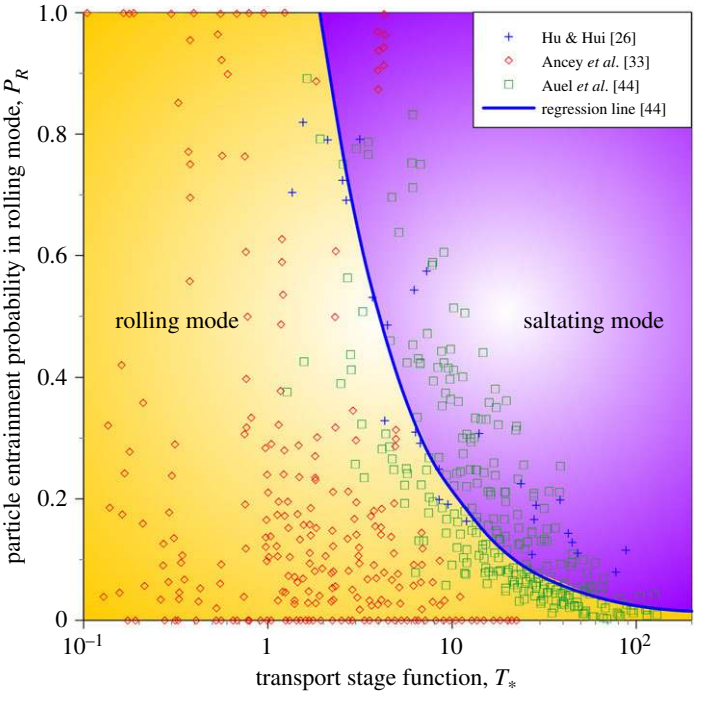

Figure 2. Particle entrainment probability P_R versus transport stage function T_* in rolling mode. (Online version in colour.)

saltation, as illustrated in figure 1, may begin as a result of particle impact against the bed and hydrodynamic lift.

Over recent decades, momentous advances in the mechanics of bed particle saltation have been primarily made through experimental observations [2,3,7,8,16–45]. In addition, several analytical and numerical studies have been carried out to model bed particle saltation [46–62]. Before going into the details of the salient features of bed particle saltation, it is rather interesting to throw some light on the threshold of bed particle saltation. Recent studies have shown that bed particle entrainment into the flow largely depends on the stochastic features of the near-bed flow, being highly sporadic in nature over a wide spectrum of spatio-temporal scales [63–66]. In the near-bed flow zone, there remain two dominant modes of particle entrainment, such as the rolling mode and saltation mode. These entrainment modes can be distinguished by introducing the *transport stage function*, which represents the excess bed shear stress ($=\tau_0-\tau_{0c}$) in non-dimensional form. The transport stage function T_* is expressed as $T_*=(\tau_0-\tau_{0c})/\tau_{0c}=(\Theta-\Theta_c)/\Theta_c$, where Θ is the Shields mobility parameter $[=u_*^2/(\Delta g d)]$, u_* is the shear velocity $[=(\tau_0/\rho_f)^{1/2}]$, ρ_f is the mass density of fluid, Δ is the submerged relative density of particles $[=(\rho_p-\rho_f)/\rho_f]$, ρ_p is the mass density of particles, g is the gravitational acceleration, Θ_c is the threshold Shields mobility parameter $[=u_{*c}^2/(\Delta g d)]$ and u_{*c} is the threshold shear velocity. The threshold Shields mobility parameter Θ_c is dependent on the particle parameter $D_*[=d(\Delta g/\nu^2)^{1/3}]$, where ν is the coefficient of kinematic viscosity of fluid. Figure 2 depicts the particle entrainment probability P_R in rolling mode as a function of transport stage function T_*. The experimental data of Hu & Hui [26], Ancey *et al*. [33] and Auel *et al*. [44] clearly indicate a decreasing trend of P_R with T_*. This suggests that, for a large transport stage function, the bed particles primarily entrain into the flow in a saltating mode. Note that Ancey *et al*. [33] reported the experimental data for both the particle entrainment probabilities, P_R and P_L, in rolling and saltating modes, respectively. In figure 2, the experimental data of P_L, given by Ancey *et al*. [33], are transformed to P_R by setting $P_R=1-P_L$. The regression line of the experimental data of Hu & Hui [26] and Auel *et al*. [44], given by $P_R=1.84T_*^{-0.94}$ [44], discriminates between the rolling

and saltation modes of particle entrainment. It therefore provides a quantitative understanding of the threshold of bed particle saltation. Auel *et al*. [44] particularly observed that, owing to the effects of particle shape, the entrainment probability of a coarse natural particle in saltating mode is larger than that of a glass sphere.

In addition to the time-averaged hydrodynamic drag F_D and lift F_L forces, bed particle saltation can begin as a result of large impulses of near-bed velocity fluctuations during the bursting events or of the effects of instantaneous hydrodynamic lift in close proximity to the bed. In addition, the hydrodynamic pressure gradient and skin friction are sources of momentum for the particles [13]. To be specific, in the rising phase of the particle trajectory, the submerged weight F_G of the particle and the vertical component of the hydrodynamic drag F_D are directed downwards (figure 1); in the recession phase, the vertical component of the hydrodynamic drag F_D being directed upwards opposes the submerged weight F_G of the particle. On the other hand, the hydrodynamic lift acting on a saltating particle is always directed upwards (normal to the particle trajectory), because the velocity of the saltating particle at a given location (elevation) is less than the flow velocity.

Experimental observations have revealed that some particles move in the form of a series of saltations [7,8,30]. This suggests that, after the particles return to the bed after performing a single saltation, they re-perform the subsequent saltation without any pause at the bed. The hydrodynamic lift remains the motivating force to lift up the particles from the bed. However, the effects of bed impact can no longer be neglected [28]. When a saltating particle collides with the bed particles, it may either rebound off the bed particles or impact against them. During the impact of the saltating particle with the bed particles, most of the particle momentum is transferred to the bed particles in a succession of horizontal impulses. This may cause a rolling motion of the surface particles in the form of surface creep [67].

Despite considerable progress in grasping the underlying mechanism of bed particle saltation both experimentally and theoretically, no review has so far been compiled in understanding the advances in the mechanics of bed particle saltation. This paper is dedicated to the current state of the art of bed particle saltation in turbulent wall-shear flow. It is arranged as follows. In §2, the mechanics of bed particle saltation is presented, including the saltation height, saltation length, particle velocity, saltation duration, particle collision with the bed, particle rotation, particle resting time and particle re-entrainment. The mathematical modelling of bed particle saltation is summarized in §3. Finally, the modelling challenges of bed particle saltation are furnished in §4, providing a new look on the bed particle saltation as a future research scope.

2. Mechanics of bed particle saltation

(a) Saltation height and saltation length

Figure 3*a* illustrates the relative saltation height h_s/d as a function of transport stage function T_*, obtained from previous experimental data [8,20,22–24,26,28,33,41,42,44]. On the other hand, figure 3*b* furnishes the experimental data of relative saltation length l_s/d as a function of transport stage function T_* [8,20,23,24,26,28,33,41,42,44]. In the insets of figure 3*a*,*b*, the schematic illustrations of bed particle saltation, highlighting the saltation height, saltation length and the reference level corresponding to the experimental data, are presented for better explanation of the phenomenon. Here, the reference level is located tangential to the summit of bed particles ($\xi = 0$). In general, the experimental data trends show that both the relative saltation height h_s/d and the relative saltation length l_s/d increase, as the transport stage function T_* increases. It is discernible that, for a given transport stage function T_*, the relative saltation height h_s/d and relative saltation length l_s/d vary over a wide range owing to the effects of particle size d and streamwise bed slope S_0. Auel *et al*. [44] reported that, for a given transport stage function $T_* = 6$, the relative saltation heights h_s/d for a mild bed slope ($S_0 = 0.01$) are approximately 1.12 times larger than those for a steep slope ($S_0 = 0.04$), whereas, for $T_* = 115$, the above differences reduce nearly to 5%. In addition, for a given transport stage function T_*, the relative saltation lengths l_s/d

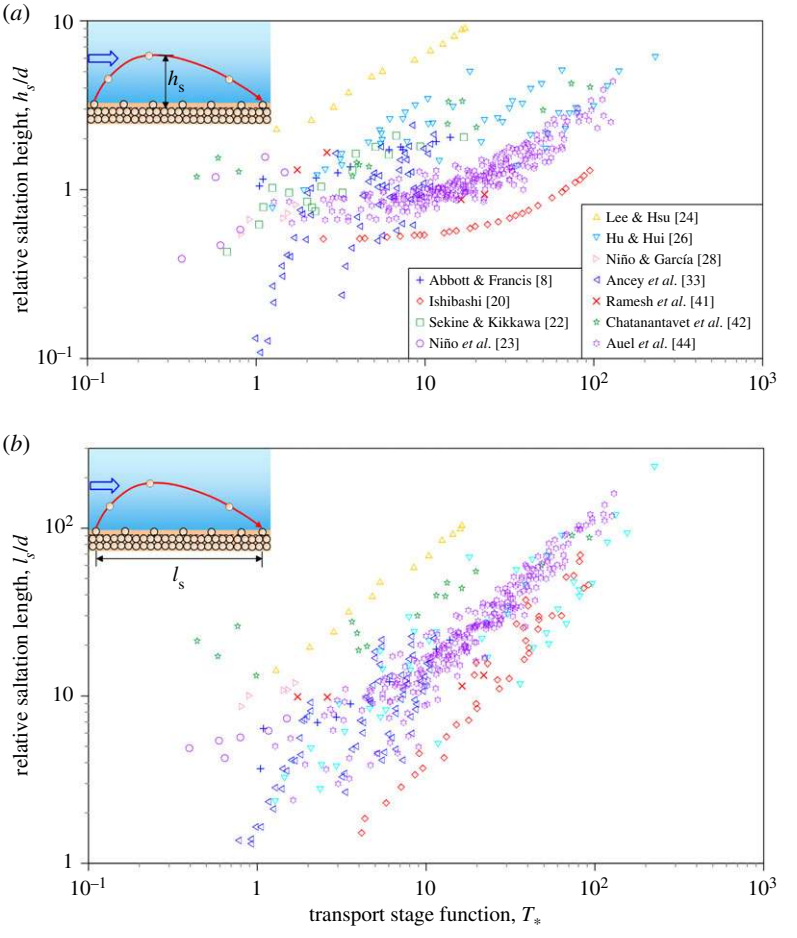

Figure 3. (*a*) Relative saltation height h_s/d versus transport stage function T_* and (*b*) relative saltation length l_s/d versus transport stage function T_*. (Online version in colour.)

for a mild bed slope ($S_0 = 0.01$) are 1.09 times larger than those for a steep slope ($S_0 = 0.04$). Auel *et al.* [44] also reported that the effects of particle shape on relative saltation height h_s/d could be prominent for coarser particles subject to a small value of T_*.

It is worth mentioning that several empirical relationships of relative saltation height h_s/d and relative saltation length l_s/d were proposed in the literature; for instance, $h_s/d = 14.3(\Theta - \Theta_c)^{0.575}$ [24]; $h_s/d = 1.78(\Delta + 1)^{0.86}\Theta^{0.69}$ [26]; $h_s/d = 0.025T_* + 0.6$ [44]; $h_s/d = 0.3D_*^{0.7}T_*^{0.5}$ [47]; $h_s/d = 1.44T_*^{0.5}$ [68] and $l_s/d = 16$ [18]; $l_s/d = 3000(u_*/w_s)^{1.5}(u_* - u_{*c})/u_*$ [22], where w_s is the terminal fall velocity of particles; $l_s/d = 2.3(T_* + 1)$ [23]; $l_s/d = 196.3(\Theta - \Theta_c)^{0.788}$ [24]; $l_s/d = 27.5(\Delta + 1)^{0.94}\Theta^{0.9}$ [26]; $l_s/d = 70(u_* - u_{*c})/w_s$ [40]; $l_s/d = 1.17T_*$ [44]; $l_s/d = 3D_*^{0.6}T_*^{0.9}$ [47]; $l_s/d = 8T_*^{0.88}$ [68]. Note that, using all the experimental data plotted in figure 3, Auel *et al.* [44] reported that $h_s/d = 0.7T_*^{0.3}$ and $l_s/d = 2.3T_*^{0.8}$. However, the empirical relationships proposed by Auel *et al.* [44] do not explicitly address the effects of particle parameter D_* on the relative saltation height h_s/d and relative saltation length l_s/d.

(b) Particle velocity

The mean particle velocity V_p in non-dimensional form can be expressed as $\mathcal{F}_d = V_p/(\Delta g d)^{1/2}$, where $\mathcal{F}_d$ is the *particle densimetric Froude number*. Figure 4 shows the experimental data of the particle densimetric Froude number $\mathcal{F}_d$ as a function of transport stage function T_* [8,16,18,22–

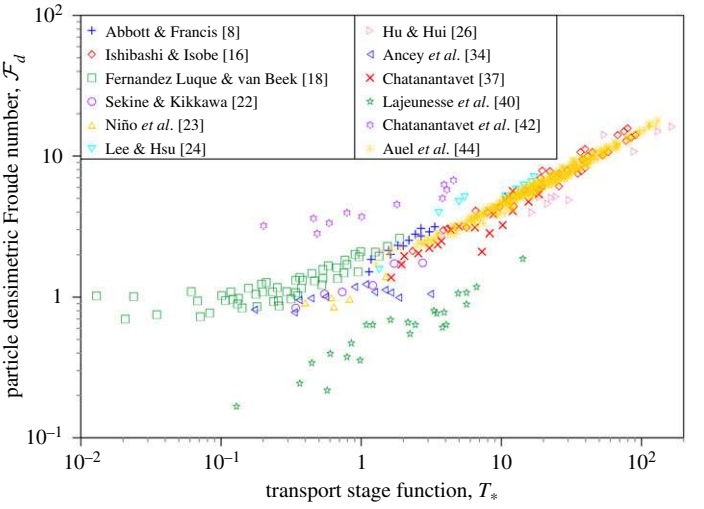

Figure 4. Particle densimetric Froude number $\mathcal{F}_d$ versus transport stage function T_*. (Online version in colour.)

24,26,34,37,40,42,44]. The experimental data display an increasing trend of particle densimetric Froude number $\mathcal{F}_d$ with transport stage function T_*. To be specific, the experimental data of Lajeunesse *et al*. [40] and Chatanantavet *et al*. [42] show considerable departure from the mean data trend. In fact, the experimental data of Lajeunesse *et al*. [40] predict lower values of particle densimetric Froude number than the mean data trend owing to the mobile bed conditions, where the particle transport can take place intermittently in both rolling and saltating modes. Conversely, the experimental data of Chatanantavet *et al*. [42] depict higher values of particle densimetric Froude number than the mean data trend, because the threshold Shields mobility parameter Θ_c in their experiments was considered to be a constant of $\Theta_c = 0.007$. However, this departure can be further reduced by modifying the threshold Shields mobility parameter Θ_c [44]. It is also evident that, for a given transport stage function T_*, the experimental data of particle densimetric Froude number $\mathcal{F}_d$ do not vary over a considerable range, excluding those of Lajeunesse *et al*. [40] and Chatanantavet *et al*. [42]. This reveals that, for a given transport stage function T_*, the effects of particle parameter D_* on particle densimetric Froude number $\mathcal{F}_d$ are not substantial. A similar conclusion is apparent from the empirical formulae of Auel *et al*. [44], van Rijn [47] and Sklar & Dietrich [68]. For the relationships of $\mathcal{F}_d$ as a function of T_*, Auel *et al*. [44] reported $\mathcal{F}_d = 1.46T_*^{0.5}$, van Rijn [47] suggested $\mathcal{F}_d = 1.5T_*^{0.6}$, while Sklar & Dietrich [68] proposed $\mathcal{F}_d = 1.56T_*^{0.56}$. In addition, several empirical formulae of mean particle velocity V_p were reported as $V_p = c_0(u_* - u_{*c})$ with c_0 = 13.4–14.3 [8], $V_p = 11.5(u_* - 0.7u_{*c})$ [18], $V_p = 8(u_*^2 - u_{*c}^2)^{0.5}$ [22], $V_p = c_1(u_* - u_{*c})$ with c_1 = 6.8–8.5 [23], $V_p = 11.53u_*(\Theta - \Theta_c)^{0.174}$ [24], $V_p = 11.9(u_* - 0.44u_{*c})$ [26] and $V_p = u_*[10 - 0.7(\Theta_c/\Theta)^{1/2}]$ [69].

(c) Saltation duration

It is interesting to shed light on how the bed particle saltation is affected by the relative submergence, which is defined as the ratio of flow depth h to particle size d. Amir *et al*. [70] particularly studied the effects of relative submergence on mean saltation duration t_s. Figure 5 shows the non-dimensional mean saltation duration $T_s(= t_s u_*/d)$ as a function of relative submergence h/d, obtained from the experimental data of researchers [23,24,26,28,70]. In general, the experimental data of non-dimensional mean saltation duration T_s appear to follow an increasing trend with the relative submergence h/d, because finer saltating particles remain for a longer duration in the fluid domain. The experimental data also indicate a clear dependency of non-dimensional mean saltation duration T_s on particle parameter D_*.

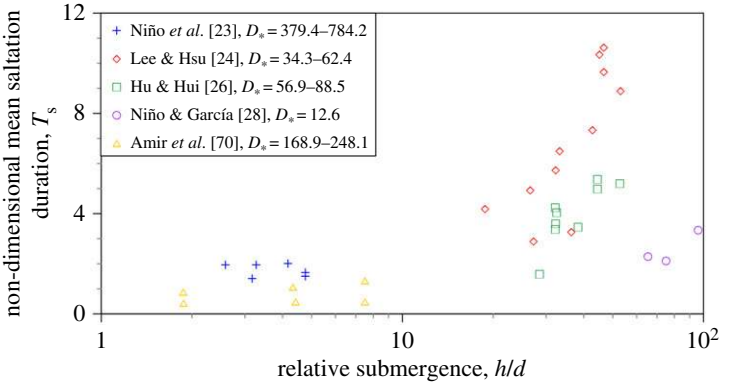

Figure 5. Non-dimensional mean saltation duration T_s versus relative submergence h/d. (Online version in colour.)

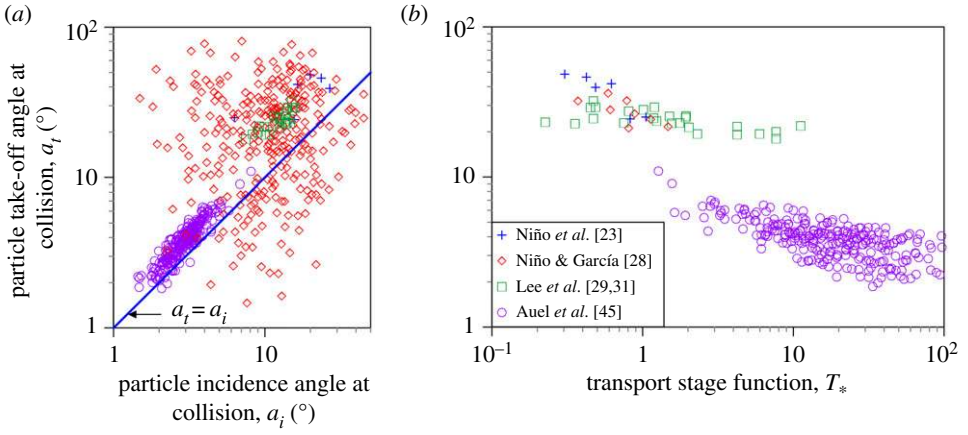

Figure 6. (*a*) Particle take-off angle a_t versus particle incidence angle a_i at collision and (*b*) particle take-off angle a_t versus transport stage function T_* at collision. (Online version in colour.)

(d) Particle collision with the bed

Particle collision with the bed remains a key feature of bed particle saltation, because the particles colliding with the bed transfer their streamwise momentum component to the normal direction to sustain the particle saltation. The characteristic parameters at collision are the particle incidence and take-off angles, a_i and a_t, and the particle incidence and take-off velocities, V_{pi} and V_{pt}, respectively (figure 1). Figure 6*a* shows the particle take-off angle a_t as a function of particle incidence angle a_i at collision, obtained from the experimental data of Niño *et al*. [23], Niño & García [28], Lee *et al*. [29,31] and Auel *et al*. [45]. From the solid line $a_t = a_i$, it turns out that, in general, the particle take-off angle at collision is larger than the particle incidence angle. This observation is largely supported by the experimental data of Niño *et al*. [23], Lee *et al*. [29,31] and Auel *et al*. [45]. Specifically, Auel *et al*. [45], who used particles of sizes in the range 5.3–18.5 mm, reported that, irrespective of particle size and particle mass density, the particle take-off angle at collision always remains larger than the particle incidence angle. However, with regard to the experimental data of Niño & García [28], who used sand particles of size 0.5 mm, the large data scatter is principally attributed to the effects of finer particle size over a wide range of flow Reynolds number. On the other hand, figure 6*b* shows the particle take-off angle a_t as a function of transport stage function T_* at collision. It is quite obvious that the particle take-off angle reduces, as the transport stage function grows, suggesting a flatter particle trajectory with an increase in transport stage function.

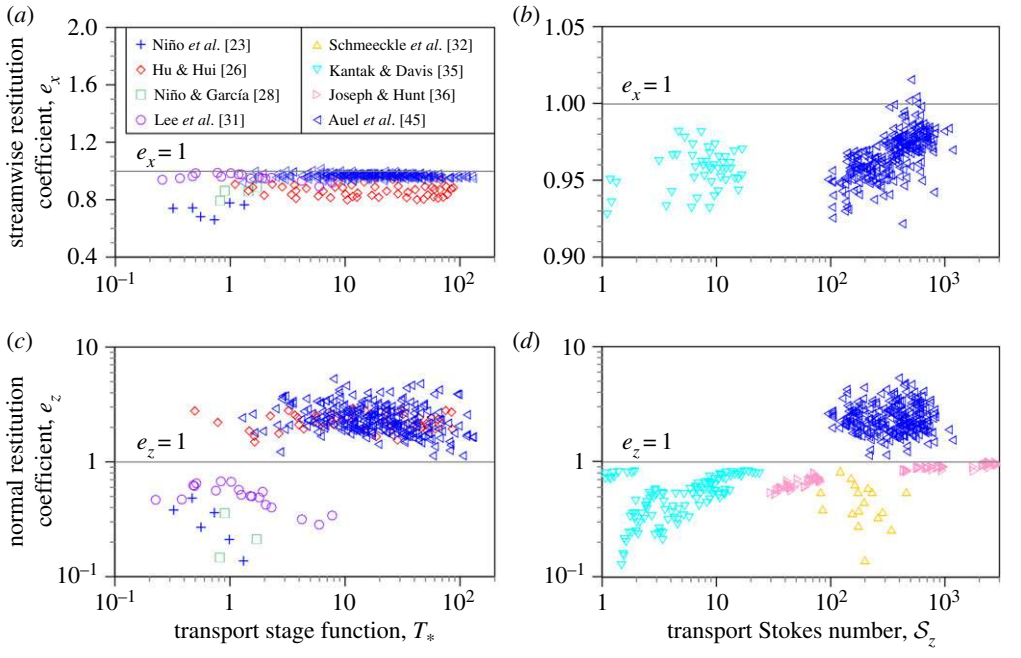

Figure 7. (*a*) Streamwise restitution coefficient e_x versus transport stage function T_*, (*b*) streamwise restitution coefficient e_x versus normal Stokes number $\mathcal{S}_z$, (*c*) normal restitution coefficient e_z versus transport stage function T_* and (*d*) normal restitution coefficient e_z versus normal Stokes number $\mathcal{S}_z$. (Online version in colour.)

The role of particle incidence and take-off velocities on bed particle saltation can be identified by introducing the streamwise and normal restitution coefficients, denoted as e_x and e_z, respectively. The e_x and e_z are expressed as

$$e_x = \frac{V_{tx}}{V_{ix}} \quad \text{and} \quad e_z = \left|\frac{V_{tz}}{V_{iz}}\right|, \tag{2.1}$$

where V_{tx} and V_{ix} are the streamwise components of particle take-off and incidence velocities at collision, respectively, and V_{tz} and V_{iz} are the normal components of particle take-off and incidence velocities at collision, respectively (figure 1).

It is pertinent to mention that the bed particle saltation after a collision with the bed depends on the *particle Stokes number*, which provides a quantitative understanding of the ratio of particle inertia to the viscous pressure force experienced by the particle [45]. The particle Stokes number $\mathcal{S}$ is expressed as

$$\mathcal{S} = \frac{2m_p V_{pi}}{3\pi \rho_f \nu d^2}, \tag{2.2}$$

where m_p is the particle mass $[= (\pi d^3/6)\rho_p]$. The normal component of the particle Stokes number (henceforth called the *normal Stokes number* for brevity) is therefore expressed as

$$\mathcal{S}_z = \mathcal{S} \sin a_i = \frac{(\Delta + 1)V_{iz} d}{9\nu}. \tag{2.3}$$

Figure 7*a* illustrates the streamwise restitution coefficient e_x as a function of transport stage function T_*, obtained from the experimental data of Niño *et al*. [23], Hu & Hui [26], Niño & García [28], Lee *et al*. [31] and Auel *et al*. [45]. On the other hand, figure 7*b* shows the experimental data of streamwise restitution coefficient e_x as a function of normal Stokes number $\mathcal{S}_z$ [35,45]. From figure 7*a*, it appears that the streamwise restitution coefficient e_x varies approximately within 0.65–1, revealing that the streamwise component of particle incidence velocity lessens after the collision. However, the variation in the mean data trend of streamwise restitution coefficient e_x

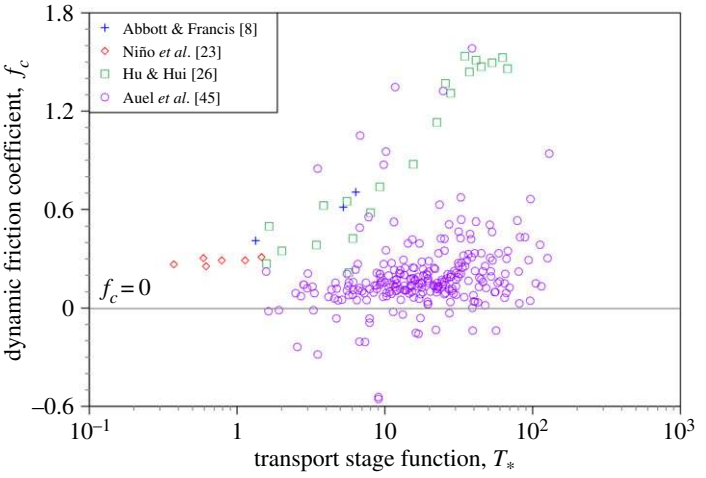

Figure 8. Dynamic friction coefficient f_c versus transport stage function T_*. (Online version in colour.)

with transport stage function T_* is trivial. By contrast, figure 7*b* shows a slight increasing trend of streamwise restitution coefficient e_x with normal Stokes number $\mathcal{S}_z$. It is evident that the e_x values are mostly below unity except at high Stokes numbers $\mathcal{S}_z$ ($\mathcal{S}_z \approx 500$–$800$), implying that the drifting force applied to the particle by the fluid is to reduce the streamwise component of particle velocity except for $\mathcal{S}_z \approx 500$–$800$. Figure 7*c* illustrates the normal restitution coefficient e_z as a function of transport stage function T_* [23,26,28,31,45]. In addition, figure 7*d* depicts the normal restitution coefficient e_z as a function of normal Stokes number $\mathcal{S}_z$ [32,35,36,45]. For a given transport stage function T_*, the normal restitution coefficient e_z varies over a significant range (figure 7*c*). The experimental data corresponding to $e_z > 1$ suggest that the normal component of particle take-off velocity is larger than the particle incidence velocity, confirming a sizable amount of momentum transfer in the normal direction to continue the next saltation step [26,45]. The normal restitution coefficient exceeding unity can be explained from the perspective of the near-bed coherent structures, which cause the particles to lift off the bed when high-momentum fluid sweeps down [45]. However, the mean data trend of normal restitution coefficient e_z varies insignificantly with the transport stage function T_*, except for a few experimental data plots [23,28,31]. On the other hand, figure 7*d* suggests an increasing trend of normal restitution coefficient e_z with normal Stokes number $\mathcal{S}_z$. It is worth noting that the normal restitution coefficients e_z, corresponding to the experimental data of Schmeeckle *et al*. [32], Kantak & Davis [35] and Joseph & Hunt [36] are less than unity, because these data were acquired in quiescent flow conditions. However, the experimental data of Auel *et al*. [45] in the range $\mathcal{S}_z = 95$–1160 (or $\mathcal{S} = 1240$–$26\,600$) show that $e_z > 1$. Note that the above range essentially crosses the threshold value of partial viscous damping, for example $\mathcal{S} = 105$ [32] and $\mathcal{S}_z \approx 100$ [36].

It is also important to find the difference between the streamwise components of particle incidence and take-off velocities. To achieve this aim, the dynamic friction coefficient f_c is often introduced. f_c is expressed as

$$f_c = \frac{(\Delta + 1)V_{ix}(V_{ix} - V_{tx})}{\Delta g l_s}. \tag{2.4}$$

Figure 8 shows the dynamic friction coefficient f_c as a function of transport stage function T_*, obtained from the experimental data reported in the literature [8,23,26,45]. The experimental data suggest that the friction coefficient f_c varies over a considerable range. The friction coefficient f_c is, in general, positive owing to the fact that $e_x < 1$, revealing that only a negligible amount of energy is transferred to the bed. However, a few experimental data of Auel *et al*. [45] contradict this traditional conclusion, showing negative values of the friction coefficient (figure 8).

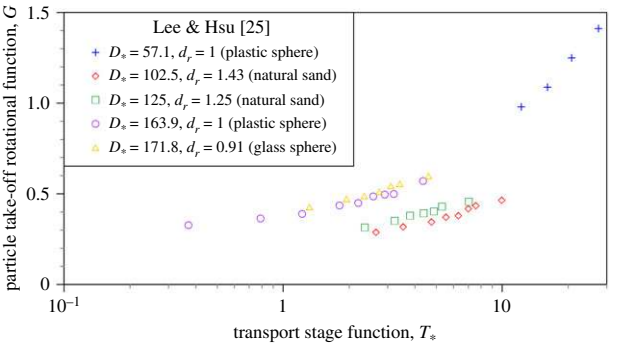

Figure 9. Particle take-off rotational function G versus transport stage function T_*. (Online version in colour.)

(e) Particle rotation

Particle rotation is principally controlled by the particle's collisions with the bed. The particle take-off angular velocity at collision is slightly larger than the particle incidence angular velocity and, subsequently, it diminishes during the next saltation step owing to the viscous effects [28]. In essence, the particle shape plays a subtle role in governing the particle angular velocity, because an elongated particle after a collision with the bed produces larger particle angular velocity than a spherical particle. The rotational motion of saltating particles was specifically studied by some researchers [25,28]. The particle rotation can be quantified by introducing the particle take-off rotational function G, which can be expressed as $G = \omega_t[d/(\Delta g)]^{1/2}$. Here, ω_t is the particle take-off angular velocity. Figure 9 shows the particle take-off rotational function G as a function of transport stage function T_*, reanalysing the experimental data of Lee & Hsu [25]. The experimental data are categorized in different classes of particle parameter D_* and relative particle size d_r, which is the ratio of saltating particle size to bed particle size. For a given particle parameter D_* and relative particle size d_r, the particle take-off rotational function G essentially increases with an increase in transport stage function T_*. This shows that the particle rotates more quickly with an increase in excess bed shear stress. Lee & Hsu [25] found that, for a given transport stage function T_*, particles with larger sizes and submerged relative densities rotate more quickly. The reason for this is ascribed to the fact that the coarse particles create intense reactive forces at collision, giving rise to rapid particle rotation. Lee & Hsu [25] also reported that a saltating particle with a relative particle size of less than unity rotates at a slower rate than that for a relative particle size equalling unity. By contrast, Niño & García [28] expressed the mean particle angular velocity Ω_m in non-dimensional form as $\hat{\Omega}_m(= \Omega_m d/u_*) = 3.98 - 1.13T_*$, implying that Ω_m decreases as T_* increases. It is contradictory to the finding of Lee & Hsu [25].

(f) Particle resting time and particle re-entrainment

The particle resting time can be defined as the time elapsed between the instant when a saltating particle comes to the bed and the instant when it continues motion. Niño & García [28] found a resting time in the range 0.3–0.7 s for sand particles of size 0.5 mm. Regaining particle motion is caused by turbulent bursting and particle–particle interactions. Experimental observations revealed the fact that, during particle transport, the ejection and sweep events remain the motivating factor towards bed particle entrainment [21,71]. In fact, the particle resting time decreases as the transport stage function increases, because the frequency of sweep events enhances with an increase in shear velocity. However, as the transport stage function increases further, the number of particles in motion per unit area and time also increases. Therefore, the resting time decreases owing to an increase in the number of re-entrainment events resulting from particle–particle interactions.

3. Modelling of bed particle saltation

(a) Deterministic approach

In the deterministic approach, the time-averaged fluid forces acting on a saltating particle are analysed. The saltating particle trajectory can be readily obtained by solving the equations of motion. The physical system is shown in figure 1, where the streambed is nearly horizontal. However, for a streambed making an inclination θ with the horizontal, the equations of motion in the xz-plane are expressed as

$$m_a\ddot{x} - F_L\frac{\dot{z}}{v_r} - F_D\frac{\bar{u}-\dot{x}}{v_r} - F_G\sin\theta - F_{Bx} = 0 \tag{3.1}$$

and

$$m_a\ddot{z} - F_L\frac{\bar{u}-\dot{x}}{v_r} + F_D\frac{\dot{z}}{v_r} + F_G\cos\theta + F_{Bz} = 0, \tag{3.2}$$

where m_a is the total particle mass including the *added fluid mass*, $(\ddot{x},\ddot{z})$ are the streamwise and normal components of particle acceleration, v_r is the particle velocity relative to the fluid flow, $\bar{u}$ is the time-averaged streamwise flow velocity, $(\dot{x},\dot{z})$ are the streamwise and normal components of particle velocity and (F_{Bx},F_{Bz}) are the streamwise and normal components of the Basset force.

As an accelerating or decelerating particle moves in a fluid, the particle moves a certain volume of neighbouring fluid, because both the particle and fluid cannot simultaneously occupy the same space. To simplify the problem, a certain volume of fluid is considered to be in motion with the particle. Therefore, the concept of added fluid mass is inevitable in modelling bed particle saltation. The total particle mass m_a is thus expressed as

$$m_a = \tfrac{1}{6}(\rho_p + \alpha_m\rho_f)\pi d^3, \tag{3.3}$$

where α_m is the added mass coefficient. In general, the added mass of a spherical particle in a potential flow can be obtained as half of the fluid mass displaced by the particle. Therefore, $\alpha_m = 0.5$ is often considered. However, the added mass coefficient in a real fluid flow differs from the idealized situation owing to the flow separation from the particle.

The hydrodynamic drag F_D acting on a particle, resulting from the pressure and the viscous skin friction effects, is expressed as

$$F_D = \tfrac{1}{8}C_D\rho_f v_r^2\pi d^2, \tag{3.4}$$

where C_D is the drag coefficient. Several empirical relationships for the drag coefficient have been proposed in the literature [13]. Specifically, van Rijn [47] used Morsi & Alexander's [72] formula, while Niño & García [49,50] used Yen's [73] formula.

On the other hand, the hydrodynamic lift on a particle can be induced in two ways. Lift due to a steep velocity gradient in the wall-shear layer is called the *Saffman lift* F_{LS} and lift due to a spinning motion of the particle is called the *Magnus lift* F_{LM}. The Saffman lift F_{LS} and the Magnus lift F_{LM} are expressed as follows [47]:

$$F_{LS} = C_L\rho_f\nu^{1/2}v_r d^2\left(\frac{\partial\bar{u}}{\partial z}\right)^{1/2} \quad \text{and} \quad F_{LM} = C_L\rho_f v_r d^3\Omega, \tag{3.5}$$

where C_L is the lift coefficient and Ω is the particle angular velocity. No consensus has so far been achieved regarding the lift coefficient C_L and, therefore, it can vary over a wide range [13].

The Basset force $\mathbf{F}_B$ takes into account the effects of temporal delay in the growth of the boundary layer adjoining the particle surface owing to the change in the relative velocity. The $\mathbf{F}_B$ is expressed as

$$\mathbf{F}_B = (F_{Bx},F_{Bz}) = \frac{3}{2}\pi^{1/2}\rho_f\nu^{1/2}d^2\int_0^t\frac{\mathrm{d}\mathbf{v_r}}{\mathrm{d}\sigma}\frac{\mathrm{d}\sigma}{(t-\sigma)^{1/2}}, \tag{3.6}$$

where $\mathbf{v_r}$ is the particle relative velocity vector, σ is the dummy variable and t is the time.

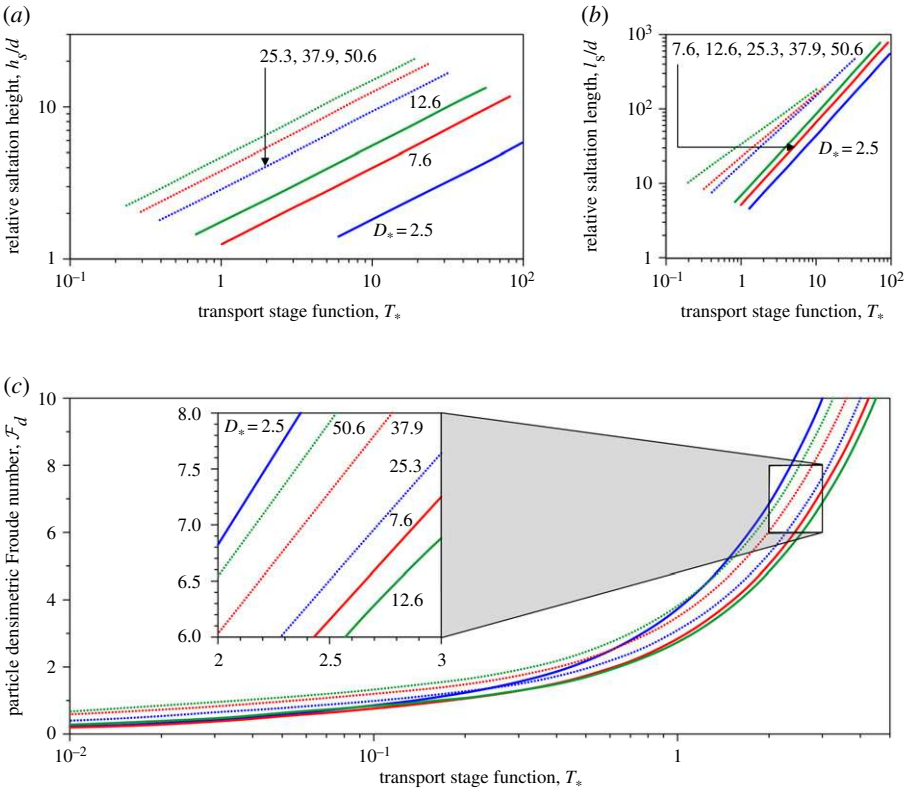

Figure 10. (*a*) Relative saltation height h_s/d versus transport stage function T_* [47], (*b*) relative saltation length l_s/d versus transport stage function T_* [47] and (*c*) particle densimetric Froude number $\mathcal{F}_d$ versus transport stage function T_* [47]. (Online version in colour.)

The submerged weight F_G of the particle is expressed as $F_G = (\pi d^3/6)\Delta\rho_f g$. Further, the streamwise flow velocity $\bar{u}$ within the wall-shear layer obeys the classical logarithmic law. The logarithmic law is expressed as

$$\bar{u} = \frac{u_*}{\kappa} \ln \frac{z}{z_0}, \tag{3.7}$$

where z_0 is the zero-velocity level. The zero-velocity level z_0 typically depends on the flow regimes, which are distinguished by the values of the shear Reynolds number $R_*(= u_* k_s/\nu)$. Here, k_s is the Nikuradse equivalent sand roughness. For a smooth flow regime ($R_* \leq 5$), $z_0 = 0.11\nu/u_*$; for a transitional flow regime ($5 < R_* < 70$), $z_0 = 0.11\nu/u_* + k_s/30$; whereas for a rough flow regime ($R_* \geq 70$), $z_0 = k_s/30$ [13].

It is worth noting that equation (3.6) is an integro-differential equation owing to the presence of the Basset force term. However, the complexity inherited by the Basset force term can be reduced following the procedure of Brush *et al.* [74]. This can transform the integro-differential equation into an ordinary differential equation. Therefore, differential equations (3.1) and (3.2) can be readily solved for a set of given parameters. Furthermore, the boundary conditions play a significant role in governing the particle trajectory. To be specific, van Rijn [47] considered the reference level to be positioned at a distance of $0.25d$ below the summit of bed particles ($\xi = 0.25$). He further considered the initial position of the saltating particle, lying on the closely packed bed particles, to be at a distance of $0.6d$ above the reference level ($\zeta = 0.6$). In addition, the initial particle velocity components were taken as $\dot{x}_0 = \dot{z}_0 = 2u_*$ [47].

Figure 10 shows the salient model results of bed particle saltation, as reported by van Rijn [47]. In figure 10*a*, the curves of relative saltation height h_s/d as a function of transport stage

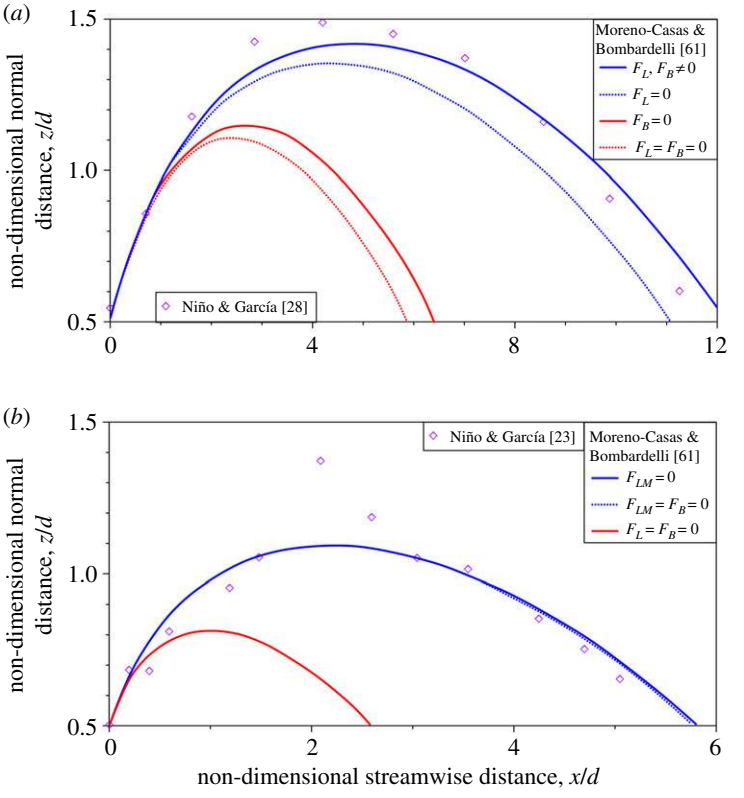

Figure 11. Comparison of the particle trajectories, obtained from the numerical simulation, with the experimental data for (*a*) $d = 0.56$ mm (sand), $u_* = 0.025\ \mathrm{ms}^{-1}$ and (*b*) $d = 30$ mm (gravel), $u_* = 0.22\ \mathrm{ms}^{-1}$. (Online version in colour.)

function T_* for different particle parameters D_* (= 2.5, 7.6, 12.6, 25.3, 37.9 and 50.6) are shown. This reveals that, for a given transport stage function T_*, the relative saltation height increases with an increase in particle size. Figure 10*b* furnishes the curves of relative saltation length l_s/d as a function of transport stage function T_* for the same set of particle parameters D_*. Similar to relative saltation height, the relative saltation length for a given transport stage function increases with an increase in particle size. On the other hand, figure 10*c* depicts the curves of particle densimetric Froude number $\mathcal{F}_d$ as a function of transport stage function T_* for different particle parameters D_*. It is apparent that, for a given transport stage function T_* smaller than unity, the particle densimetric Froude number $\mathcal{F}_d$ insignificantly varies with the particle parameter D_*. The enlarged frame bounded by $T_* \in [2, 3]$ and $\mathcal{F}_d \in [6, 8]$ clearly shows the dependency of the particle parameter D_* on the particle densimetric Froude number $\mathcal{F}_d$.

It is worth emphasizing that, with regard to the sediment transport studies, the consideration of the Basset force in the equations of motion was generally overlooked [24,47,75]. However, it was revealed that the Basset force plays an important role for finer particles [50,61]. To be specific, the Basset force plays an effective role in the case of sand saltation rather than gravel saltation. For the sand saltation, Moreno-Casas & Bombardelli [61] reported that, when the Basset force is ignored in the numerical simulation, the saltation length and the saltation height, obtained from the analysis, underestimate the experimental data by 40% and 15%, respectively.

Figure 11*a*,*b* illustrates the comparison of the particle saltation trajectories, obtained from the numerical simulation, with the experimental data for sand and gravel, respectively. For various combinations of hydrodynamic forces, the model results anticipate the utmost importance of the hydrodynamic lift and the Basset force. It is also apparent that, for sand saltation (figure 11*a*), the Basset force must be taken into account to accurately predict the particle saltation trajectory.

(b) Computational fluid dynamics approach

The major drawback of the theoretical models based on the deterministic approach is that they are unable to address the fluctuations in particle trajectories induced by the near-bed coherent structures. In addition, the deterministic approach of bed particle saltation cannot anticipate the subtle effects of bed packing conditions on the saltation characteristics. With the advent of high-resolution computational fluid dynamics schemes, impressive strides have been made in understanding the interaction between the particle motion and the near-bed coherent structures [76,77]. Such an interaction gives rise to the formation of various sediment patterns that could be predicted through numerical simulations [78,79]. For turbulent flow over a regular array of fixed spherical particles, Chan-Braun *et al*. [80] applied direct numerical simulation (DNS) in conjunction with the immersed boundary method (IBM) for the turbulent flow and the fluid–particle interaction, respectively. They particularly examined the hydrodynamic forces and torques on the bed particles. Some studies applied the artificial repulsion potential to determine the particle–particle collisions and the subsequent contact forces, neglecting the tangential friction [76,81]. This assumption could affect the particle rotation and in turn the Magnus lift. Ji *et al*. [77] specifically investigated particle entrainment by the turbulent flow, combining DNS, the IBM and the finite-discrete element method (FDEM), which could effectively model the particle motion and particle–particle collisions. The numerical results revealed a close association of the continuous particle saltation with the sweep events. In addition, they showed that the pressure gradients rather than the shear stresses play a decisive role in governing the particle dynamics.

In another attempt, Ji *et al*. [57] studied bed particle saltation in a rough bed comprising closely packed spherical particles, coupling DNS, the IBM and the FDEM. The numerical simulation revealed that, in the near-bed flow zone, the entrained particles substantially modify the profiles of flow velocity and turbulent stresses. In essence, the quasi-streamwise oriented fluid streaks do not originate in the vicinity of the bed. However, far from the bed, the coherent structures are retrieved owing to the trivial effects of bed roughness and particle–particle collisions in the outer flow zone. The continuous bed particle saltation obtained from the numerical simulation evidenced the collision-rebounding mechanism. The link between the quick changes in particle streamwise and normal velocity components uncovered the fact that the transfer of the particle streamwise momentum component to the normal direction is guided by the particle's collision with the bed. This mechanism is quite different from that of bed particle entrainment, where the particle normal momentum component is received from the coherent structures. Very recently, bed particle saltation was studied by coupling large eddy simulation (LES) and the discrete element model (DEM) [82,83]. Liu *et al*. [83] reported that the saltating particle trajectory is primarily driven by turbulent fluctuations and the particle's collisions with the bed. The particle velocity components in the streamwise and normal directions obey a skewed Gaussian distribution. In addition, the turbulent fluctuations can somewhat enhance the correlation between the particle incidence and take-off angles.

(c) Determination of bedload flux

Figure 12*a* shows a schematic illustration of bedload flux in a continuum scale, whereas figure 12*b* illustrates the motion of a single particle with a mean saltation length of l_s. The bedload flux q_b (in volume per unit time and bed width) can be defined as the product of the mean particle velocity V_p, the volumetric particle concentration C within the bedload layer and the bedload layer thickness δ_b. The δ_b can be approximately considered as the saltation height h_s. Therefore, q_b is expressed as

$$q_b = V_p C h_s. \tag{3.8}$$

Importantly, using experimental data, van Rijn [47] expressed the volumetric particle concentration C within the bedload layer as $C = 0.18 C_0 T_*/D_*$, where C_0 is the maximum bedload concentration, which can be taken as 0.65 [47]. The bedload flux q_b in non-dimensional form, called the *bedload flux function*, is expressed as $\Phi_b = q_b/(\Delta g d^3)$. Therefore, using equation (3.8), the

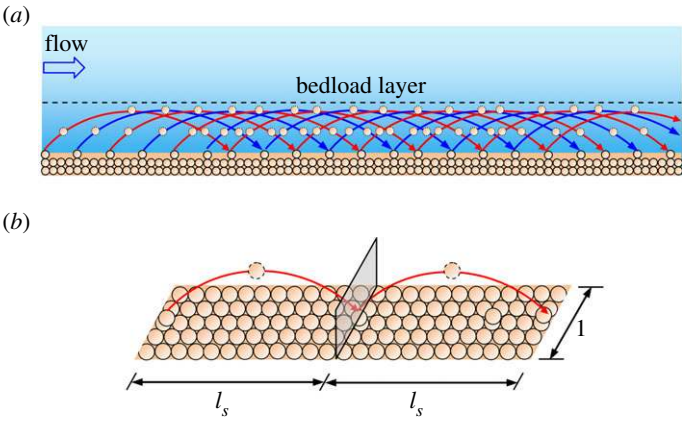

Figure 12. Schematic illustration of (*a*) bedload flux and (*b*) motion of a single particle with a mean saltation length of l_s. (Online version in colour.)

Φ_b is expressed as

$$\Phi_b = \mathcal{F}_d C \frac{h_s}{d}. \tag{3.9}$$

Using several empirical relationships for the particle densimetric Froude number $\mathcal{F}_d$ and the relative saltation height h_s/d as mentioned earlier, the bedload flux function can be evaluated from equation (3.9).

On the other hand, the bedload flux g_{bs} can also be defined in terms of submerged weight per unit time and bed width. The g_{bs} is expressed as $g_{bs} = W_b V_p$ [50], where W_b is the submerged weight per unit bed area. Considering the dynamic friction coefficient f_c (see equation (2.4)), the W_b is expressed as $W_b = \tau_{0p}/f_c$, where τ_{0p} is the dispersive particle shear stress. Following the concept of Bagnold [84], the applied bed shear stress τ_0 can be decomposed into the dispersive particle shear stress τ_{0p} and the interfacial fluid shear stress τ_{0f}, implying $\tau_0 = \tau_{0p} + \tau_{0f}$. Bagnold [84] argued that, at the equilibrium condition, the interfacial fluid shear stress τ_{0f} equals the threshold bed shear stress τ_{0c}. This results in $\tau_{0p} = \tau_0 - \tau_{0c}$. Thus, the W_b takes the form $W_b = (\tau_0 - \tau_{0c})/f_c$. The bedload flux g_{bs} (in submerged weight per unit time and bed width) is then expressed as

$$g_{bs} = \frac{\tau_0 - \tau_{0c}}{f_c} V_p. \tag{3.10}$$

Therefore, the bedload flux function Φ_b reads

$$\Phi_b = \mathcal{F}_d \frac{\Theta - \Theta_c}{f_c}. \tag{3.11}$$

Importantly, equation (3.11) expresses the bedload flux function Φ_b as a function of the excess Shields mobility parameter ($= \Theta - \Theta_c$) and the particle densimetric Froude number $\mathcal{F}_d$. Using equation (2.4) for the dynamic friction coefficient f_c and several empirical relationships for the particle densimetric Froude number $\mathcal{F}_d$, the bedload flux function can be estimated from equation (3.11).

The bedload flux can also be determined from the entrainment probability of a particle in saltating mode. The entrainment probability P_L in saltating mode is expressed as the hydrodynamic lift exceeding the submerged weight of the particle, implying $P_L = P_L(F_L \geq F_G)$. Einstein [4,5] considered that, during bedload transport, the particles move in a series of brief jumps in succession. The average saltation length was considered to be λ_s times the particle diameter ($l_s = \lambda_s d$), where λ_s for spherical particles is 100. However, later Einstein [5] modified the average saltation length by introducing the entrainment probability in saltating mode. Since P_L denotes the probability of hydrodynamic lift exceeding the submerged weight, this suggests

that the number of particles that deposit on the bed after performing a saltation length is $N(1-P_L)$, where N is the number of particles in motion. Therefore, NP_L particles remain in motion. Consequently, $NP_L(1-P_L)$ particles deposit on the bed and NP_L^2 particles continue to move after travelling the second step. In this way, the process continues until all the particles deposit on the bed after a given time. Thus, the average saltation length l_s (symbol remains the same for brevity) can be expressed as

$$l_s = \sum_{N=0}^{\infty} (1-P_L)P_L^N(N+1)\lambda_s d = \lambda_s d(1-P_L)^{-1}. \tag{3.12}$$

If g_b denotes the bedload flux in dry weight per unit time and bed width and i_{bs} represents the bedload fraction to be deposited for a given particle size, then the particle deposition rate per unit time and bed width is $g_b i_{bs}$. It follows that the number of particles N_d deposited per unit time and bed area is $N_d = g_b i_{bs}(1-P_L)/(l_x \rho_p g k_1 d^3) = g_b i_{bs}(1-P_L)/(\lambda_s \rho_p g k_1 d^4)$, where k_1 is a factor accounting for the particle volume.

On the other hand, if i_{br} represents the bedload fraction to be removed for a given particle size, then the number of such particles per unit bed area is $i_{br}/(k_2 d^2)$, where k_2 accounts for the projected area of the particle. Therefore, the number of particles N_r removed per unit time and bed area is $N_r = [i_{br}/(k_2 d^2)] \times (P_L/t_e)$, where t_e is the exchange time. Einstein [5] considered the exchange time t_e to be proportional to d/w_s, where w_s follows $w_s \propto (\Delta g d)^{1/2}$. This suggests $t_e = k_3 d/w_s$, where k_3 is a proportionality constant. At an equilibrium condition, the particle deposition rate is balanced by the particle removal rate. Therefore, equating N_d and N_r results in

$$\Phi_{b*} = A_*^{-1} P_L (1-P_L)^{-1}, \tag{3.13}$$

where $\Phi_{b*} = \Phi_b \times (i_{bs}/i_{br})$ and $A_* = k_2 k_3/(k_1 \lambda_s)$.

Einstein [5] considered the lift force fluctuations $\eta(t)$ to obey the Gaussian distribution and expressed the lift force fluctuations in non-dimensional form as $\eta_* = \eta(t)/\eta_0$, where η_0 is a constant (= 0.5). Following the condition: $P_L = P_L(F_L \geq F_G)$, Einstein expressed the entrainment probability P_L in saltating mode as

$$P_L = 1 - \frac{1}{\pi^{1/2}} \int_{-B_* \Psi_{b*} - \eta_0^{-1}}^{B_* \Psi_{b*} - \eta_0^{-1}} \exp(-t^2)\, \mathrm{d}t, \tag{3.14}$$

where $B_* = B/[\eta_0 \ln^2(10.6)]$, $B = 2k_1\kappa^2/(k_2 C_L)$, κ is the von Kármán constant (= 0.41), $\Psi_{b*} = [\Psi_b' \xi_h Y \ln^2(10.6)]/\beta_x^2$, Ψ_b' is the flow intensity function due to particle roughness [$= \Delta d/(R_b' S_0)$], R_b' is the hydraulic radius due to particle roughness, ξ_h is the hiding coefficient, Y is the lift correction factor, $\beta_x = \ln(10.6X/\Delta_k)$, X is the characteristic bed particle size ($X = 0.77\Delta_k$ for $\Delta_k/\delta_v \geq 1.8$ and $X = 1.39\delta_v$ for $\Delta_k/\delta_v < 1.8$), Δ_k is the apparent roughness ($= k_s/x_k$), x_k is a correction factor and δ_v is the viscous sublayer thickness. Einstein [5] considered the lift coefficient C_L to be 0.178. Equation (3.13) provides an estimation of the bedload flux function as a function of entrainment probability in saltating mode, which can be determined from equation (3.14).

Engelund & Fredsøe [69] expressed the bedload flux g_b (in dry weight per unit time and bed width) as $g_b = (\pi d^3/6)\rho_p g(P_L/d^2)V_p$, where the P_L was obtained following the concept of Bagnold [84] as $P_L = 6(\Theta - \Theta_c)/(\pi f_c)$. They finally obtained the bedload flux function Φ_b as

$$\Phi_b = \frac{9.3}{f_c}(\Theta - \Theta_c)(\Theta^{1/2} - 0.7\Theta_c^{1/2}). \tag{3.15}$$

In this context, it is worth noting that these researchers obtained the entrainment probability in saltating mode by analysing the hydrodynamic forces at the particle scale. A detailed description of the mathematical analyses of bed particle entrainment was reviewed elsewhere [66]. Importantly, Dey & Ali [65] determined the bedload flux on a continuum scale by extending the mathematical analysis at the particle scale. Dey & Ali [65] expressed the number of entrained particles N per unit bed width during a time period $\mathrm{d}t$ as $N = [4A_b/(\pi d^2)]P_L C_b$, where A_b is the bed surface area with a unit bed width ($= l_s \times 1$). As the saltation length l_s increases with an increase in time-averaged hydrodynamic lift F_L and reduces with an increase in submerged

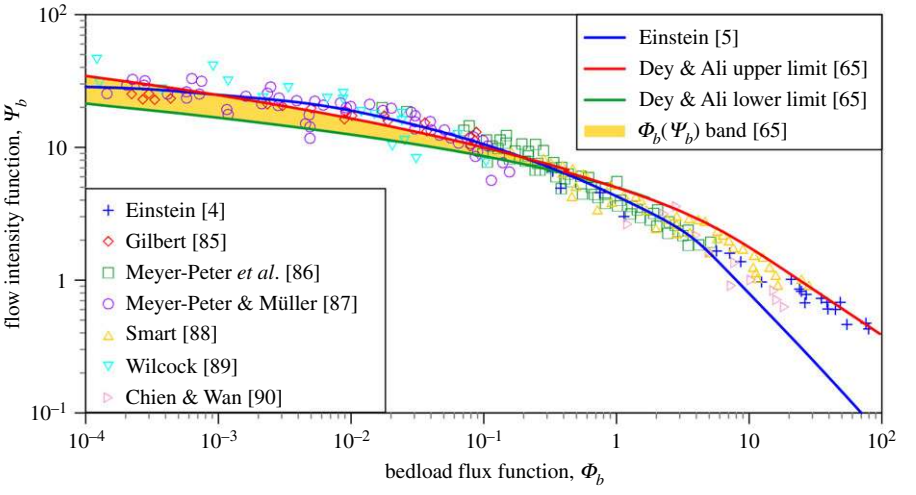

Figure 13. Bedload flux function Φ_b versus flow intensity function Ψ_b. (Online version in colour.)

weight F_G of particle, it follows that $l_s/d \propto F_L/F_G$. Using the expressions for F_L and F_G, Dey & Ali [65] obtained $l_s/d = k_4 C_L \Theta(u^{+2} + \sigma_u^{+2})$, where k_4 is a coefficient including the added mass coefficient, u^+ is $\bar{u}/u_*$, σ_u^+ is σ_u/u_*, σ_u is the streamwise turbulence intensity $[= (\overline{u'u'})^{1/2}]$ and u' is the fluctuations of instantaneous streamwise flow velocity from its time-averaged value. The time period $\mathrm{d}t$ for particle removal from the bed was considered to be $\mathrm{d}t = k_5 d/u_*$, where k_5 is a coefficient. Dey & Ali [65] expressed the bedload flux g_b as $g_b = (N/\mathrm{d}t)\rho_p g(\pi d^3/6)$ and finally obtained the bedload flux function Φ_b as

$$\Phi_b = K_6 C_b C_L P_L (u^{+2} + \sigma_u^{+2}) \Psi_b^{-3/2}, \tag{3.16}$$

where k_6 is a coefficient that was found to be 4.5 and Ψ_b is the flow intensity function $(= \Theta^{-1})$.

Figure 13 shows the bedload flux function Φ_b as a function of flow intensity function Ψ_b, obtained from the model of Dey & Ali [65]. In addition, the $\Phi_b(\Psi_b)$ curve of Einstein [5] and ample experimental data of researchers [4,85–90] are furnished. Dey & Ali [65] specifically provided the dependency of the $\Phi_b(\Psi_b)$ curve on particle size d. The upper and lower limits of the $\Phi_b(\Psi_b)$ curves of Dey & Ali [65] correspond to the particle sizes d = 0.8 and 4 mm, respectively. It turns out that the Dey and Ali upper and lower limiting curves are frozen curves, which do not vary for $d < 0.8$ mm and $d > 4$ mm, respectively, revealing that the dependency of the $\Phi_b(\Psi_b)$ curve on particle size d only persists in the domain $d \in [0.8, 4]$ mm.

4. Closure

Bed particle saltation in turbulent wall-shear flow, studied over recent decades, has been thoroughly reviewed in the light of experimental observations, highlighting the relevant features of the mechanics of particle saltation. In addition, the mathematical modelling of bed particle saltation has been critically appraised, discussing the roles of the near-bed hydrodynamic forces and the turbulence. The determination of bedload flux, stemming from the mathematical modelling of bed particle saltation, has also been elaborated. Despite significant advances in the experimental observations on bed particle saltation, a unique mathematical model of bed particle saltation in turbulent wall-shear flow remains in its infancy. The reason for this is attributed to the lack of construction of a generalized force system that is capable of capturing the essential elements of the fluid–particle and particle–particle interactions.

One of the major drawbacks of the existing mathematical models of bed particle saltation turns out to be a strong conjecture stating that the flow field is hardly affected by the particle motion.

In fact, the fluid flow drives the particle motion and, in turn, the particle motion modifies the fluid flow [91]. Experimental observations have demonstrated that, for a mobile bed, the velocity laws in the near-bed flow zone are essentially modified, revealing a departure of the von Kámán constant from its well-accepted value (= 0.41) in flow over a rigid bed [92]. Therefore, a proper coupling between the fluid flow and the particle motion needs further thought. In addition, the identification of hydrodynamic drag and lift forces on a moving particle in the near-bed flow zone requires attention. This is because of the fact that, in addition to the time-averaged hydrodynamic drag and lift forces, the effects of velocity fluctuations play a prominent role in sustaining bed particle saltation. The form-induced drag on a particle, generated by the streamwise advective acceleration, can no longer be ignored in the theoretical analysis. Further, the turbulent lift force, resulting from the vertical velocity fluctuations that arise from the vertical advective acceleration, must be included in the mathematical model. The effects of particle size on bed particle saltation have been well explored experimentally. However, to model bed particle saltation in a gravel-bed stream, appropriate constitutive relationships supporting a large corpus of experimental data are yet to be developed in analysing the force system. Furthermore, in mathematical modelling, the consideration of the effects of particle–particle collisions away from the bed on the dynamics of bed particle saltation is far from complete [93]. Among the key features of bed particle saltation, little attempt has so far been made to probe the role of the hydrodynamic impulse on the initiation of bed particle saltation. These important issues must be accounted for in the mathematical modelling of bed particle saltation not only to mirror this natural phenomenon but also to reconcile theory and practice. Therefore, further research is required to build a promising model of bed particle saltation by addressing the aforementioned issues.

Data accessibility. This paper does not have any additional data.

Authors' contributions. The authors of this paper contributed jointly.

Competing interests. We declare we have no competing interests.

Funding. No funding has been received for this article.

Acknowledgements. S.D. acknowledges the JC Bose Fellowship in pursuing this work. We are thankful to Christian Auel for providing us with experimental data [44,45].

References

1. Bagnold RA. 1937 The transport of sand by wind. *Geogr. J.* **89**, 409–438. (doi:10.2307/1786411)
2. Bagnold RA. 1956 The flow of cohesionless grains in fluids. *Phil. Trans. R. Soc. Lond. A* **249**, 235–297. (doi:10.1098/rsta.1956.0020)
3. Bagnold RA. 1973 The nature of saltation and of 'bedload' transport in water. *Proc. R. Soc. Lond. A* **332**, 473–504. (doi:10.1098/rspa.1973.0038)
4. Einstein HA. 1942 Formulas for the transportation of bed load. *Trans. Am. Soc. Civ. Eng.* **107**, 561–577.
5. Einstein HA. 1950 The bed-load function for sediment transportation in open channel flows. Technical bulletin 1026, United States Department of Agriculture, Soil Conservation Service, Washington, DC, USA.
6. Owen PR. 1964 Saltation of uniform grains in air. *J. Fluid Mech.* **20**, 225–242. (doi:10.1017/S0022112064001173)
7. Francis JRD. 1973 Experiments on the motion of solitary grains along the bed of a water-stream. *Proc. R. Soc. Lond. A* **332**, 443–471. (doi:10.1098/rspa.1973.0037)
8. Abbott JE, Francis JRD. 1977 Saltation and suspension trajectories of solid grains in a water stream. *Phil. Trans. R. Soc. Lond. A* **284**, 225–254. (doi:10.1098/rsta.1977.0009)
9. Anderson RS, Haff PK. 1988 Simulation of eolian saltation. *Science* **241**, 820–823. (doi:10.1126/science.241.4867.820)
10. Maegley WJ. 1976 Saltation and Martian sandstorms. *Rev. Geophys.* **14**, 135–142. (doi:10.1029/RG014i001p00135)
11. Greeley R, Marshall JR. 1985 Transport of Venusian rolling 'stones' by wind? *Nature* **313**, 771–773. (doi:10.1038/313771a0)
12. Bridges NT, Ayoub F, Avouac J-P, Leprince S, Lucas A, Mattson S. 2012 Earth-like sand fluxes on Mars. *Nature* **485**, 339–342. (doi:10.1038/nature11022)

13. Dey S. 2014 *Fluvial hydrodynamics: hydrodynamic and sediment transport phenomena*. Berlin, Germany: Springer.
14. Ali SZ, Dey S. 2016 Mechanics of advection of suspended particles in turbulent flow. *Proc. R. Soc. A* **472**, 20160749. (doi:10.1098/rspa.2016.0749)
15. Dey S, Ali SZ, Padhi E. 2018 Advances in analytical modeling of suspended sediment transport. *J. Hydro-environ. Res.* **20**, 110–126. (doi:10.1016/j.jher.2018.02.004)
16. Ishibashi T, Isobe A. 1968 Hydraulic study on the protection of erosion of sand flush channel. Report 67104. Central Research Institute of Electric Power Industry (CRIEPI), Tokyo, Japan. [In Japanese.]
17. Gordon R, Carmichael JB, Isackson FJ. 1972 Saltation of plastic balls in a 'one-dimensional' flume. *Water Resour. Res.* **8**, 444–459. (doi:10.1029/WR008i002p00444)
18. Fernandez Luque R, van Beek R. 1976 Erosion and transport of bed-load sediment. *J. Hydraul. Res.* **14**, 127–144. (doi:10.1080/00221687609499677)
19. Murphy PJ, Hooshiari H. 1982 Saltation in water dynamics. *J. Hydraul. Div.* **108**, 1251–1267.
20. Ishibashi T. 1983 A hydraulic study on protection for erosion of sediment flush equipments of dams. *Proc. JSCE* **1983**, 103–112. [In Japanese.] (doi:10.2208/jscej1969.1983.334_103)
21. Drake TG, Shreve RL, Dietrich WE, Whiting PJ, Leopold LB. 1988 Bedload transport of fine gravel observed by motion-picture photography. *J. Fluid Mech.* **192**, 193–217. (doi:10.1017/S0022112088001831)
22. Sekine M, Kikkawa H. 1992 Mechanics of saltating grains. II. *J. Hydraul. Eng.* **118**, 536–558. (doi:10.1061/(ASCE)0733-9429(1992)118:4(536))
23. Niño Y, García M, Ayala L. 1994 Gravel saltation: 1 Experiments. *Water Resour. Res.* **30**, 1907–1914. (doi:10.1029/94WR00533)
24. Lee H-Y, Hsu I-S. 1994 Investigation of saltating particle motions. *J. Hydraul. Eng.* **120**, 831–845. (doi:10.1061/(ASCE)0733-9429(1994)120:7(831))
25. Lee H-Y, Hsu I-S. 1996 Particle spinning motion during saltating process. *J. Hydraul. Eng.* **122**, 587–590. (doi:10.1061/(ASCE)0733-9429(1996)122:10(587))
26. Hu C, Hui Y. 1996 Bed-load transport. *J. Hydraul. Eng.* **122**, 245–254. (doi:10.1061/(ASCE)0733-9429(1996)122:5(245))
27. Hu C, Hui Y. 1996 Bed-load transport. II: Stochastic characteristics. *J. Hydraul. Eng.* **122**, 255–261. (doi:10.1061/(ASCE)0733-9429(1996)122:5(255))
28. Niño Y, García M. 1998 Experiments on saltation of sand in water. *J. Hydraul. Eng.* **124**, 1014–1025. (doi:10.1061/(ASCE)0733-9429(1998)124:10(1014))
29. Lee H-Y, Chen Y-H, You J-Y, Lin Y-T. 2000 Investigations of continuous bed load saltating process. *J. Hydraul. Eng.* **126**, 691–700. (doi:10.1061/(ASCE)0733-9429(2000)126:9(691))
30. Lee H-Y, You J-Y, Lin Y-T. 2002 Continuous saltating process of multiple sediment particles. *J. Hydraul. Eng.* **128**, 443–450. (doi:10.1061/(ASCE)0733-9429(2002)128:4(443))
31. Lee H-Y, Lin Y-T, You J-Y, Wang H-W. 2006 On three-dimensional continuous saltating process of sediment particles near the channel bed. *J. Hydraul. Res.* **44**, 374–389. (doi:10.1080/00221686.2006.9521689)
32. Schmeeckle MW, Nelson JM, Pitlick J, Bennett JP. 2001 Interparticle collision of natural sediment grains in water. *Water Resour. Res.* **37**, 2377–2391. (doi:10.1029/2001WR000531)
33. Ancey C, Bigillon F, Frey P, Lanier J, Ducret R. 2002 Saltating motion of a bead in a rapid water stream. *Phys. Rev. E* **66**, 036306 doi:10.1103/PhysRevE.66.036306)
34. Ancey C, Davison AC, Böhm T, Jodeau M. 2008 Entrainment and motion of coarse particles in a shallow water stream down a steep slope. *J. Fluid Mech.* **595**, 83–114. (doi:10.1017/S0022112007008774)
35. Kantak AA, Davis RH. 2004 Oblique collisions and rebound of spheres from a wetted surface. *J. Fluid Mech.* **509**, 63–81. (doi:10.1017/S0022112004008900)
36. Joseph GG, Hunt ML. 2004 Oblique particle–wall collisions in a liquid. *J. Fluid Mech.* **510**, 71–93. (doi:10.1017/S002211200400919X)
37. Chatanantavet P. 2007 Physically-based models of bedrock incision processes in mountain streams. PhD thesis, University of Minnesota, Minneapolis, MN, USA.
38. Wang H-W, Lee H-Y, Lee P-N. 2009 Three-dimensional saltating processes of multiple sediment particles. *Int. J. Sedim. Res.* **24**, 16–32. (doi:10.1016/S1001-6279(09)60013-5)
39. Hill KM, DellAngelo L, Meerschaert MM. 2010 Heavy-tailed travel distance in gravel bed transport: an exploratory enquiry. *J. Geophys. Res. Earth Surf.* **115**, F00A14. (doi:10.1029/2009JF001276)

40. Lajeunesse E, Malverti L, Charru F. 2010 Bed load transport in turbulent flow at the grain scale: experiments and modeling. *J. Geophys. Res. Earth Surf.* **115**, F04001. (doi:10.1029/2009JF001628)
41. Ramesh B, Kothyari UC, Murugesan K. 2011 Near-bed particle motion over transitionally-rough bed. *J. Hydraul. Res.* **49**, 757–765. (doi:10.1080/00221686.2011.620369)
42. Chatanantavet P, Whipple KX, Adams MA, Lamb MP. 2013 Experimental study on coarse grain saltation dynamics in bedrock channels. *J. Geophys. Res. Earth Surf.* **118**, 1161–1176. (doi:10.1002/jgrf.20053)
43. Naqshband S, McElroy B, Mahon RC. 2017 Validating a universal model of particle transport lengths with laboratory measurements of suspended grain motions. *Water Resour. Res.* **53**, 4106–4123. (doi:10.1002/2016WR020024)
44. Auel C, Albayrak I, Sumi T, Boes RM. 2017 Sediment transport in high-speed flows over a fixed bed: 1. Particle dynamics. *Earth Surf. Proc. Landf.* **42**, 1365–1383. (doi:10.1002/esp.4128)
45. Auel C, Albayrak I, Sumi T, Boes RM. 2017 Sediment transport in high-speed flows over a fixed bed: 2. Particle impacts and abrasion prediction. *Earth Surf. Proc. Landf.* **42**, 1384–1396. (doi:10.1002/esp.4132)
46. White BR, Schultz JC. 1977 Magnus effect in saltation. *J. Fluid Mech.* **81**, 497–512. (doi:10.1017/S0022112077002183)
47. van Rijn LC. 1984 Sediment transport, part I: bed load transport. *J. Hydraul. Eng.* **110**, 1431–1456. (doi:10.1061/(ASCE)0733-9429(1984)110:10(1431))
48. Wiberg PL, Smith JD. 1985 A theoretical model for saltating grains in water. *J. Geophys. Res. Oceans* **90**, 7341–7354. (doi:10.1029/JC090iC04p07341)
49. Niño Y, García M. 1994 Gravel saltation: 2. Modeling. *Water Resour. Res.* **30**, 1915–1924. (doi:10.1029/94WR00534)
50. Niño Y, García M. 1998 Using Lagrangian particle saltation observations for bedload sediment transport modelling. *Hydrol. Process.* **12**, 1197–1218. (doi:10.1002/(SICI)1099-1085(19980630)12:8<1197::AID-HYP612>3.0.CO;2-U)
51. Nikora V, Heald J, Goring D, McEwan I. 2001 Diffusion of saltating particles in unidirectional water flow over a rough granular bed. *J. Phys. A: Math. Gen.* **34**, L743–L749. (doi:10.1088/0305-4470/34/50/103)
52. Heald J, McEwan I, Tait S. 2004 Sediment transport over a flat bed in a unidirectional flow: simulations and validation. *Phil. Trans. R. Soc. A* **362**, 1973–1986. (doi:10.1098/rsta.2004.1426)
53. Bialik RJ. 2011 Particle–particle collision in Lagrangian modelling of saltating grains. *J. Hydraul. Res.* **49**, 23–31. (doi:10.1080/00221686.2010.543778)
54. Bialik RJ. 2011 Numerical study of saltation of non-uniform grains. *J. Hydraul. Res.* **49**, 697–701. (doi:10.1080/00221686.2011.598025)
55. Moreno PA, Bombardelli FA. 2012 3D Numerical simulation of particle-particle collisions in saltation mode near stream beds. *Acta Geophys.* **60**, 1661–1688. (doi:10.2478/s11600-012-0077-x)
56. Bialik RJ, Czernuszenko W. 2013 On the numerical analysis of bed-load transport of saltating grains. *Int. J. Sedim. Res.* **28**, 413–420. (doi:10.1016/S1001-6279(13)60051-7)
57. Ji C, Munjiza A, Avital E, Xu D, Williams J. 2014 Saltation of particles in turbulent channel flow. *Phys. Rev. E* **89**, 052202. (doi:10.1103/PhysRevE.89.052202)
58. Maldonado S, Borthwick AGL. 2015 Sensitivity analysis and statistical convergence of a saltating particle model. *J. Hydraul. Eng.* **141**, 04014091. (doi:10.1061/(ASCE)HY.1943-7900.0000987)
59. Bialik RJ. 2015 Lagrangian modelling of saltating sediment transport: a review. In *Rivers—physical, fluvial and environmental processes* (eds P Rowiński, A Radecki-Pawlik), pp. 427–441. Berlin, Germany: Springer.
60. Bialik RJ, Nikora VI, Karpiński M, Rowiński PM. 2015 Diffusion of bedload particles in open-channel flows: distribution of travel times and second-order statistics of particle trajectories. *Environ. Fluid Mech.* **15**, 1281–1292. (doi:10.1007/s10652-015-9420-5)
61. Moreno-Casas PA, Bombardelli FA. 2016 Computation of the Basset force: recent advances and environmental flow applications. *Environ. Fluid Mech.* **16**, 193–208. (doi:10.1007/s10652-015-9424-1)
62. Chen Y, Bai Y, Xu D. 2017 On the mechanisms of the saltating motion of bedload. *Int. J. Sedim. Res.* **32**, 53–59. (doi:10.1016/j.ijsrc.2016.07.001)

63. Ali SZ, Dey S. 2016 Hydrodynamics of sediment threshold. *Phys. Fluids* **28**, 075103. (doi:10.1063/1.4955103)
64. Dey S, Ali SZ. 2017 Stochastic mechanics of loose boundary particle transport in turbulent flow. *Phys. Fluids* **29**, 055103. (doi:10.1063/1.4984042)
65. Dey S, Ali SZ. 2017 Mechanics of sediment transport: particle scale of entrainment to continuum scale of bedload flux. *J. Eng. Mech.* **143**, 04017127. (doi:10.1061/(ASCE)EM.1943-7889.0001343)
66. Dey S, Ali SZ. 2018 Review article: advances in modeling of bed particle entrainment sheared by turbulent flow. *Phys. Fluids* **30**, 061301. (doi:10.1063/1.5030458)
67. Zhang Y, Wang Y, Yang B, Jia P. 2016 Measurement of sand creep on a flat sand bed using a high speed digital camera: mesoscopic features of creeping grains. *Sedimentology* **63**, 629–644. (doi:10.1111/sed.12232)
68. Sklar LS, Dietrich WE. 2004 A mechanistic model for river incision into bedrock by saltating bed load. *Water Resour. Res.* **40**, W06301. (doi:10.1029/2003WR002496)
69. Engelund F, Fredsøe J. 1976 A sediment transport model for straight alluvial channels. *Nord. Hydrol.* **7**, 293–306. (doi:10.2166/nh.1976.0019)
70. Amir M, Nikora V, Witz M. 2017 A novel experimental technique and its application to study the effects of particle density and flow submergence on bed particle saltation. *J. Hydraul. Res.* **55**, 101–113. (doi:10.1080/00221686.2016.1233583)
71. Niño Y, García MH. 1996 Experiments on particle–turbulence interactions in the near-wall region of an open channel flow: implications for sediment transport. *J. Fluid Mech.* **326**, 285–319. (doi:10.1017/S0022112096008324)
72. Morsi SA, Alexander AJ. 1972 An investigation of particle trajectories in two-phase flow systems. *J. Fluid Mech.* **55**, 193–208. (doi:10.1017/S0022112072001806)
73. Yen BC. 1992 Sediment fall velocity in oscillating flow. Water Resources and Environmental Engineering Research Report, issue 11. Department of Civil Engineering, University of Virginia, Charlottesville, VA, USA.
74. Brush LM, Ho H-W, Yen B-C. 1964 Accelerated motion of a sphere in a viscous fluid. *J. Hydraul. Div.* **90**, 149–160.
75. Schmeeckle MW, Nelson JM. 2003 Direct numerical simulation of bedload transport using a local, dynamic boundary condition. *Sedimentology* **50**, 279–301. (doi:10.1046/j.1365-3091.2003.00555.x)
76. Shao X, Wu T, Yu Z. 2012 Fully resolved numerical simulation of particle-laden turbulent flow in a horizontal channel at a low Reynolds number. *J. Fluid Mech.* **693**, 319–344. (doi:10.1017/jfm.2011.533)
77. Ji C, Munjiza A, Avital E, Ma J, Williams JJR. 2013 Direct numerical simulation of sediment entrainment in turbulent channel flow. *Phys. Fluids* **25**, 056601. (doi:10.1063/1.4807075)
78. Kidanemariam AG, Uhlmann M. 2014 Direct numerical simulation of pattern formation in subaqueous sediment. *J. Fluid Mech.* **750**, R2. (doi:10.1017/jfm.2014.284)
79. Kidanemariam AG, Uhlmann M. 2017 Formation of sediment patterns in channel flow: minimal unstable systems and their temporal evolution. *J. Fluid Mech.* **818**, 716–743. (doi:10.1017/jfm.2017.147)
80. Chan-Braun C, García-Villalba M, Uhlmann M. 2011 Force and torque acting on particles in a transitionally rough open-channel flow. *J. Fluid Mech.* **684**, 441–474. (doi:10.1017/jfm.2011.311)
81. Kidanemariam AG, Chan-Braun C, Doychev T, Uhlmann M. 2013 Direct numerical simulation of horizontal open channel flow with finite-size, heavy particles at low solid volume fraction. *New J. Phys.* **15**, 025031. (doi:10.1088/1367-2630/15/2/025031)
82. Elghannay H, Tafti D. 2018 LES-DEM simulations of sediment transport. *Int. J. Sedim. Res.* **33**, 137–148. (doi:10.1016/j.ijsrc.2017.09.006)
83. Liu D, Liu X, Fu X. 2019 LES-DEM simulations of sediment saltation in a rough-wall turbulent boundary layer. *J. Hydraul. Res.* **57**, 1–12. (doi:10.1080/00221686.2018.1509384)
84. Bagnold RA. 1954 Experiments on a gravity-free dispersion of large solid spheres in a Newtonian fluid under shear. *Proc. R. Soc. Lond. A* **255**, 49–63. (doi:10.1098/rspa.1954.0186)
85. Gilbert GK. 1914 The transportation of debris by running water. Professional paper no. 86. United States Geological Survey, Washington, DC, USA.
86. Meyer-Peter E, Favre H, Einstein HA. 1934 Neuere Versuchsresultate über den Geschiebetrieb. *Schweizerische Bauzeitung* **103**, 147–150.

87. Meyer-Peter E, Müller R. 1948 Formulas for bed-load transport. In *Proc. of the 2nd Meeting of the Int. Assoc. for Hydraulic Research, Stockholm, Sweden, 7–9 June 1948*, vol. 3, pp. 39–64. Madrid, Spain: IAHR.
88. Smart GM. 1984 Sediment transport formula for steep channels. *J. Hydraul. Eng.* **110**, 267–276. (doi:10.1061/(ASCE)0733-9429(1984)110:3(267))
89. Wilcock PR. 1988 Methods for estimating the critical shear stress of individual fractions in mixed-size sediment. *Water Resour. Res.* **24**, 1127–1135. (doi:10.1029/WR024i007p01127)
90. Chien N, Wan Z. 1999 *Mechanics of sediment transport*. Reston, VA: ASCE Press, American Society of Civil Engineers.
91. McEwan IK, Jefcoate BJ, Willetts BB. 1999 The grain–fluid interaction as a self-stabilizing mechanism in fluvial bed load transport. *Sedimentology* **46**, 407–416. (doi:10.1046/j.1365-3091.1999.00197.x)
92. Dey S, Das R, Gaudio R, Bose SK. 2012 Turbulence in mobile-bed streams. *Acta Geophys.* **60**, 1547–1588. (doi:10.2478/s11600-012-0055-3)
93. Leeder MR. 1979 'Bedload' dynamics: grain–grain interactions in water flows. *Earth Surf. Proc. Landf.* **4**, 229–240. (doi:10.1002/esp.3290040304)